Supporting Information for

Ultrafast Intraband Spectroscopy of

Hot-Carrier Cooling in Lead-Halide Perovskites

Thomas R. Hopper[†], Andrei Gorodetsky[†], Jarvist M. Frost[‡¶], Christian Müller[§#], Robert Lovrincic[§#] and Artem A. Bakulin[†]*

† Department of Chemistry, Imperial College London, London SW7 2AZ, United Kingdom

‡ Department of Materials, Imperial College London, London, SW7 2AZ, United Kingdom

⊥Department of Physics, Imperial College London, London, SW7 2AZ, United Kingdom

¶ Department of Physics, King's College London, London, WC2R 2LS, United Kingdom

§ Institute for High-Frequency Technology, Technische Universität Braunschweig, Schleinitzstr. 22, 38106, Braunschweig, Germany

InnovationLab, Speyerer Str. 4, 69115, Heidelberg, Germany

* E-mail: a.bakulin@imperial.ac.uk

Experimental

Materials. All films were spin-coated from solution on CaF_2 substrates in a nitrogen atmosphere. Prior to deposition, the substrates were treated with a mild oxygen plasma to improve wetting. $CsPbBr_3$ was spin-coated from DMSO solution, while $FAPbBr_3$, $MAPbBr_3$, $FAPbI_3$, and $MAPbI_3$ were spin-coated from mixed DMSO+DMF solutions. The anti-solvent technique was used to improve crystallization (1 ml toluene before the end of spin-coating). The samples were subsequently slowly annealed on a hot plate in a nitrogen atmosphere. We determined the film thicknesses via spectroscopic ellipsometry ($FAPbI_3$ 450 nm, $MAPbI_3$ 500 nm, $FAPbBr_3$ 500 nm, $MAPbBr_3$ 500 nm, $CsPbBr_3$ 300nm).

Optical characterization. UV-Vis absorption spectra were obtained for the perovskite films on CaF_2 using a Shimadzu 2600 spectrometer equipped with an ISR-2600Plus integrating sphere attachment. The slit width was 5 nm and the sampling interval was 1 nm.

Ultrafast optical spectroscopy. A 4 kHz Ti:sapphire regenerative amplifier (Astrella, Coherent) provided seed pulses (800 nm, ~35 fs) to two optical parametric amplifiers (TOPAS-Prime, Coherent). The pump energy was selected by tuning the signal output of "TOPAS 1" and the articulation of a beta-barium borate crystal as appropriate. The NIR idler output (0.6 eV) of "TOPAS 2" was split into two paths; ~90% of the intensity was used as the push, and the remaining ~10% was used as the probe. The pump was modulated at 2 kHz by an optical chopper, and the time delays of the pump and probe were controlled using mechanical delay stages. The pump and probe adopted a collinear geometry, with the push beam travelling on a separate optical path. The pump and probe beams were directed to a ~200 μm diameter spot on the sample using a 10 cm concave mirror. The push was slightly defocused to facilitate beam overlap and prevent

photodegradation of the sample, and blocked completely for pump-probe measurements. For each material system, at least three spots on two separate films were measured. The sample was housed in a N_2-purged quartz cuvette during measurements. Changes to the transmission of the probe were detected by an amplified PbSe photodetector (PDA20H-EC, ThorLabs), coupled to a lock-in amplifier (SR830, Stanford Research Systems).
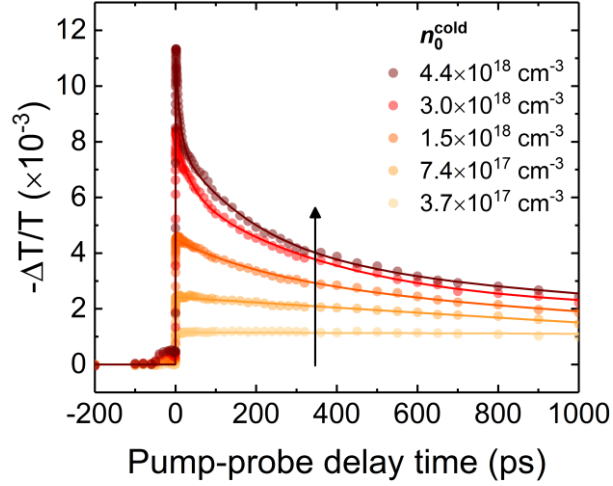
Figure S1. *Fluence-dependent pump-probe kinetics for MAPbI₃. n_0^{cold} is the initial cold charge carrier density. Pump: 2.06 eV; probe: 0.6 eV. Multiexponential fits provide a guide to the eye.*
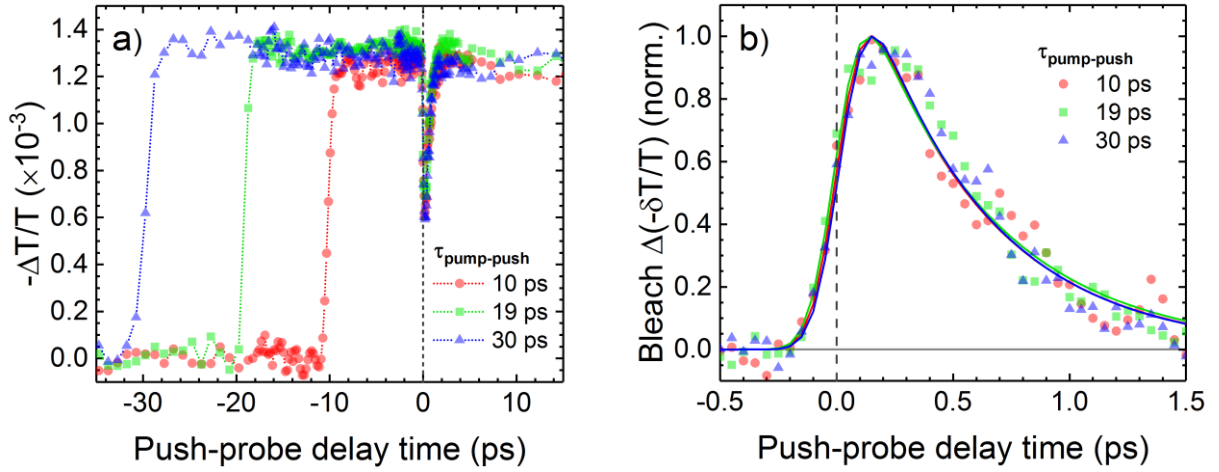
Figure S2. *PPP transients for MAPbI₃, with different pump-push delay times. The pump, push and probe energies are 1.9, 0.54 and 0.54 eV. The pump and push fluence were fixed at 32 μJ cm⁻² and 2.4 mJ cm⁻² in all cases. (a) For a fixed push-probe delay, the pump arrival time was altered. (b) For each of the PPP transients, the recovery of the push-induced bleaching displays the same kinetics. Solid lines are Gaussian-convoluted monoexponential fits.*
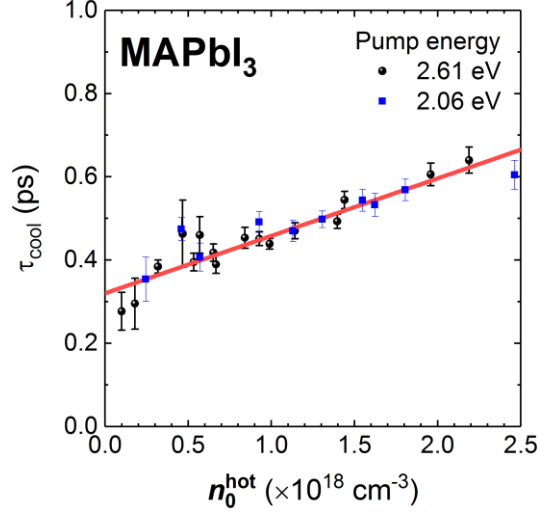
Figure S3. *Hot-carrier cooling time (τ_{cool}) plotted as a function of the initial hot-carrier density (n_0^{hot}) for MAPbI$_3$, with different pump energies. The linear regression (red line) applied to the data obtained with the 2.61 eV pump (excess energy ~1 eV) also appears to fit the data obtained with the lower energy pump (2.06 eV, excess energy ~0.5 eV).*
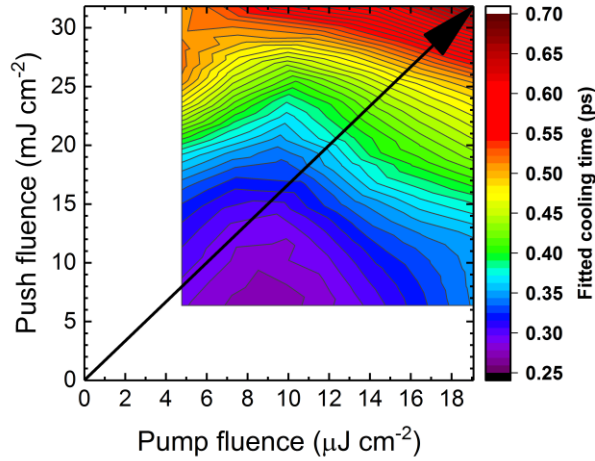
Figure S4. *Pseudocolour map describing the effect of both the pump and push fluence (and, by extension, the respective cold- and hot-carrier densities) on the fitted hot-carrier cooling time (τ_{cool}) of a CsPbBr$_3$ film. Pump: 2.6 eV; push: 0.6 eV; probe: 0.6 eV. The solid arrow represents the linear relationship between the pump and push fluence on τ_{cool}; $\tau_{cool} \propto J_{pump} \cdot J_{push}$.*

Theory

The polaron theories used in this work require a material parametrization based on an effective-mass approximation for the electronic structure, and a single harmonic dielectrically coupled phonon mode with no band dispersion (i.e. flat).

The band-structure influenced parameters (effective mass, and optical dielectric constant) were set to constants based on the halogen in the perovskite (i.e. the same for different cations), to make the trend due to phonon parameters more clear. Due to the heavy atoms involved, the electronic structure must include relativistic effects (spin-orbit coupling), and the materials are moderately correlated requiring a beyond mean-field (such as density functional theory) technique. We used effective masses for the iodide perovskites of 0.12 electron masses, and for the bromide perovskites a 20% enhancement of this, 0.144, by analogy with the trend in the tin halide perovskites.[1]

Optical dielectric constants are dependent on the details of the higher-lying excited states, and subtle band-gap renormalizations due to exciton effects. Careful measurements of high quality films are likely to be more reliable than electronic structure calculations. We use the refractive indices measured on single crystals with ellipsometry as our reference.[2] (In particular, see the digital supplementary information data file, where the refractive indices are listed on the first line. The optical dielectric constant is, naturally, the square of the refractive index.)

Material-specific properties were calculated by plane-wave pseudo-potential density functional theory, in the VASP code. Explicit d-orbitals were used in the electronic structure for the Pb and Sn atoms. The PBE-sol generalized gradient approximation was used, with a 700 eV cutoff for the plane-wave basis. Pseudo-cubic unit cells of the materials were geometry-relaxed with a conjugate

gradient method. Phonons at the Γ-point of the Brillouin zone were calculated with density functional perturbation theory. Combined with born-effective-charges at the same level of theory, these eigenvectors were used to calculate the infrared activity of these modes, and thereby the total ionic dielectric response.

The material-specific phonon frequencies, infrared activities and ionic dielectric constants were then combined with the halogen-specific optical dielectric constant and effective masses to fully specify the polaron model for each material. These data were then used with the PolaronMobility.jl codes,[3] to calculate the polaron state and associated transient behavior – most particularly the Kadanoff polaron optical-mode scattering time. Custom codes were written to sum the phonon frequency (energy) over a Bose-Einstein distribution in order to calculate the per-unit cell heat capacity at 300 K.[4]

Table S1. Table of parameters used for the polaron theory calculations, with the Polaronmobility.jl codes.[3] To enable cross comparison and focus on the effect of phonons, consistent halogen-specific electronic parameters (effective mass and optical dielectric constant) were used for all the bromide- and iodide-perovskites. Effective mass, m*, in units of electron mass. Effective LO phonon frequency, $f_{effective}$, from infrared activity of phonon modes by the Hellwarth et al. 'B' scheme.[5] Optical dielectric constant, ε_{optic}, set as a halogen-specific value, from a measurement of refractive index by ellipsometry.[2] A material-specific ionic contribution to the dielectric constant, ε_{ion}, from summing over the infrared active phonon modes at the Γ-point of the Brillouin zone (DFPT calculation). $\alpha_{Fröhlich}$, the dimensionless dielectric electron-phonon coupling can be calculated from these preceding values. Specific heat capacity, from the energy

of the Γ-point modes, and summing with a Bose-Einstein distribution at 300 K, a per-unit cell specific heat capacity can be estimated. Small variations between different materials are due to mode stiffening and softening. The much smaller specific heat capacity for the inorganic material is due to there being only half as many low-energy cage modes. Introduction of a non-spherical organic ion breaks the symmetry, and doubles the number of modes. This we associate inversely with the slope of the change in cooling rate with fluence. Polaron scattering time. The polaron Feynman variational parameters (υ and ω)[6] are calculated for the above polaron model, with a free-energy (finite temperature) at 300 K. From this model, the finite-temperature Kadanoff mobility theory[7] can be used to obtain a polaron scattering time (also evaluated at 300 K). This we associated with the zero-fluence extrapolated rate of cooling: the cooling is limited by the rate of scattering into the dielectrically coupled optical phonon modes. The polaron radius can be calculated directly from the υ variational parameter in the finite-temperature Feynman polaron model, and is the width of the polaron (Gaussian) wavefunction.

	$FAPbI_3$	$MAPbI_3$	$FAPbBr_3$	$MAPbBr_3$	$CsPbBr_3$
m*	0.12	0.12	0.144	0.144	0.144
$f_{effective}$ (THz)	1.71	2.25	1.31	2.37	3.06
ε_{optic}	5.61	5.61	4.16	4.16	4.16
ε_{ion}	22.9	15.4	33.8	15.9	10.0
$\alpha_{Fröhlich}$	2.18	1.73	4.07	2.69	2.11
Specific heat capacity (meV)	303.5	347.3	375.3	339.5	204.7
Polaron scattering time (ps), at 300 K	0.158	0.167	0.095	0.098	0.110
Polaron radius (Å)	22.9	31.6	13.7	26.2	36.0

References

(1)   Huang, L.-y.; Lambrecht, W. R. L. Electronic Band Structure, Phonons, and Exciton Binding Energies of Halide Perovskites $CsSnCl_3$, $CsSnBr_3$, and $CsSnI_3$. *Phys. Rev. B* **2013,** *88* (16), 165203-165203.
(2)   Leguy, A. M. A.; Azarhoosh, P.; Alonso, M. I.; Campoy-Quiles, M.; Weber, O. J.; Yao, J.; Bryant, D.; Weller, M. T.; Nelson, J.; Walsh, A. et al. Experimental and Theoretical Optical Properties of Methylammonium Lead Halide Perovskites. *Nanoscale* **2016,** *8* (12), 6317-6327.
(3)   Frost, J. M. Polaronmobility.Jl: Implementation of the Feynman Variational Polaron Model. *Journal of Open Source Software* **2018,** *3* (28), 566-566.
(4)   2018-05-Hopper-Polaron-Cooling.   https://doi.org/10.5281/zenodo.1400794   (accessed 21/08/2018).
(5)   Hellwarth, R. W.; Biaggio, I. Mobility of an Electron in a Multimode Polar Lattice. *Phys. Rev. B* **1999,** *60* (1), 299-307.
(6)   Feynman, R. P. Slow Electrons in a Polar Crystal. *Phys. Rev.* **1955,** *97* (3), 660-665.
(7)   Kadanoff, L. P. Boltzmann Equation for Polarons. *Phys. Rev.* **1963,** *130* (4), 1364-1369.